Aristolochic Acid Nephropathy as a Potential Model of Renal Senescence

Shingo Urate
Department of Medical Science and Cardiorenal Medicine, Yokohama City University Graduate School of Medicine, Yokohama

Hiromichi Wakui (hiro1234@yokohama-cu.ac.jp)
Department of Medical Science and Cardiorenal Medicine, Yokohama City University Graduate School of Medicine, Yokohama

Kengo Azushima
Department of Medical Science and Cardiorenal Medicine, Yokohama City University Graduate School of Medicine, Yokohama

Takahiro Yamaji
Cardiovascular and Metabolic Disorders Program, Duke-NUS Medical School

Toru Suzuki
Department of Medical Science and Cardiorenal Medicine, Yokohama City University Graduate School of Medicine, Yokohama

Eriko Abe
Department of Medical Science and Cardiorenal Medicine, Yokohama City University Graduate School of Medicine, Yokohama

Shohei Tanaka
Department of Medical Science and Cardiorenal Medicine, Yokohama City University Graduate School of Medicine, Yokohama

Shinya Taguchi
Department of Medical Science and Cardiorenal Medicine, Yokohama City University Graduate School of Medicine, Yokohama

Shunichiro Tsukamoto
Department of Medical Science and Cardiorenal Medicine, Yokohama City University Graduate School of Medicine, Yokohama

Sho Kinguchi
Department of Medical Science and Cardiorenal Medicine, Yokohama City University Graduate School of Medicine, Yokohama

Kazushi Uneda
Department of Medical Science and Cardiorenal Medicine, Yokohama City University Graduate School of Medicine, Yokohama

Tomohiko Kanaoka

Department of Medical Science and Cardiorenal Medicine, Yokohama City University Graduate School of Medicine, Yokohama

Yoshitoshi Atobe

Department of Neuroanatomy, Yokohama City University School of Medicine, Yokohama

Kengo Funakoshi

Department of Neuroanatomy, Yokohama City University School of Medicine, Yokohama

Akio Yamashita

Department of Investigative Medicine, Graduate School of Medicine, University of the Ryukyus, Okinawa

Kouichi Tamura

Department of Medical Science and Cardiorenal Medicine, Yokohama City University Graduate School of Medicine, Yokohama

---

Research Article

Keywords: chronic kidney disease, aristolochic acid, aging

Posted Date: June 18th, 2021

DOI: https://doi.org/10.21203/rs.3.rs-620317/v1

Abstract

The kidney is among the organs most susceptible to age-associated impairments. Although there has recently been extensive research on renal aging, appropriate models remain limited. Generally, renal aging is strongly associated with renal fibrosis, which is the final common pathway of chronic kidney disease. Aristolochic acid (AA), a nephrotoxic agent, causes aristolochic acid nephropathy (AAN), characterized by progressive renal fibrosis and functional decline. Here, we examined the potential of AAN as a model of renal senescence by chronically administering AA to C57BL/6 mice. Compared with controls, the AA group presented aged kidney-like phenotypes such as renal atrophy, renal functional decline, and tubulointerstitial fibrosis. Additionally, AA promoted cellular senescence specifically in the kidney, concomitant with increase in renal p16 mRNA expression and senescence-associated β-galactosidase activity. Furthermore, AA-treated mice exhibited proximal tubular mitochondrial abnormalities, followed by accumulation of reactive oxygen species. Additionally, Klotho, an antiaging gene, was significantly decreased in the kidney of AA-treated mice. Collectively, the results of the present study indicate that AAN partially mimics the aged kidney and may serve as a useful mouse model for research on renal aging.

Introduction

With the continuous increase in lifespan, more individuals are suffering from age-related impairments. The kidney is a typical target organ of age-associated tissue damage, and the incidence of chronic kidney disease increases with age[1]. Furthermore, renal aging accelerates overall aging, which results in shortening of lifespan. Therefore, research on renal aging is necessary, although appropriate animal models have not been fully developed. Renal aging is accompanied with various pathological changes including renal atrophy, glomerulosclerosis, and tubulointerstitial fibrosis[2]. Notably, renal tubulointerstitial fibrosis is a final common pathway in most forms of progressive renal disease, which suggests that renal fibrosis is closely associated with the aged kidney.

In research on aging, mice are used as a reliable tool because of their genetic proximity to humans, the possibility to genetically manipulate their genome, and the fact that they present similar aging-related phenotypes as humans during their lifespan[3]. Longitudinal observations using inbred mice are ideal as a model of aging, although it is time-consuming to follow mice for their full lifespan. Additionally, there are several genetically modified mouse models of aging. The Klotho-deficient mouse is a model of premature aging that can be used for research on aging. However, renal function is unaffected in this model, which may lead to difficulties in evaluating renal alterations that result from premature aging[4].

Aristolochic acid (AA) stimulation causes renal injury known as aristolochic acid nephropathy (AAN) that is characterized by extensive interstitial fibrosis. AA is toxic primarily to renal tubular epithelium by forming DNA adducts in renal tissues[5]. Although AAN is often accompanied by urothelial malignancy, AA is unlikely to affect organs outside the urinary system and may be appropriate for evaluating kidney-specific alterations. Therefore, AA is commonly employed to establish a model of renal fibrosis in mice. This model is relatively easy to establish as AA is injected intraperitoneally. In the present study, we

hypothesized that AA accelerates age-related alterations in the kidney, and the age-related features of AAN were investigated.

Results

AA administration induced significant weight loss and renal atrophy.

Baseline body weight (BW) and systolic blood pressure (BP) were identical between the vehicle control and AA groups. BW in the vehicle control group increased consistently for 8 weeks. In contrast, weight gain was inhibited during the AA stimulation period, and BW was significantly lower in the AA group at 4 and 8 weeks after AA administration (Fig. 1A). Regarding BP and heart rate, there were no significant differences between the AA and vehicle control groups (Fig. 1B and C). Heart weight/body weight ratio showed no difference (Fig. 1D), although the kidney weight/body weight ratio was significantly lower in the AA group (Fig. 1E).

AA administration induced significant renal functional decline.

We next examined renal function in the vehicle control and AA groups. Plasma creatinine concentration and urea nitrogen were significantly higher in the AA group compared with the vehicle control group. Additionally, AA treatment significantly reduced creatinine clearance compared with the vehicle control group (Fig. 2A-C). Histological examination using periodic acid-Schiff (PAS) staining revealed that glomerular area was significantly decreased in the AA group compared with the vehicle control group (Fig. 2D).

AA administration induced overt tubulointerstitial fibrosis and significant upregulation of fibrosis-related gene expression in the kidney.

Extensive tubulointerstitial fibrosis, assessed using Masson’s trichrome staining, was observed in the AA group (Fig. 3A), concomitant with upregulation of mRNA pertaining to the renal fibrosis-related genes, collagen I and III, and transforming growth factor (TGF)-β (Fig. 3B-D).

AA administration accelerated cellular senescence in the kidney.

To evaluate cellular senescence, we examined renal expression of p53, p21, p16, and glutaminase (GLS) mRNA. The AA group demonstrated significantly higher mRNA levels of these senescence-related genes in the kidney (Fig. 4A-D). Furthermore, senescence-associated β-galactosidase (SA-β-gal) staining in the kidney was increased in the AA group, while there was virtually none in the vehicle control group (Fig. 4E).

AA administration induced mitochondrial dysfunction and accumulation of reactive oxygen species in the kidney.

In the AA group exclusively, electron microscopic observation revealed disappearance of mitochondrial cristae, mitochondrial fragmentation, cytoplasmic vacuolization, and autolysosomes in proximal tubular

cells, concomitant with downregulation of BCL2/adenovirus E1B 19-kDa interacting protein 3 (Bnip3), a mitochondria-related gene (Fig. 5A and B). Renal mRNA expression of Nox2, a component of NADPH oxidases, was significantly increased in the AA group compared with the vehicle control group (Fig. 5C). Furthermore, western blot revealed 4-hydroxy-2-nonenal (4-HNE) level was significantly increased in the kidney of the AA group (Fig. 5D). These results indicated that AA administration induced cellular senescence, mitochondrial dysfunction, and accumulation of reactive oxygen species (ROS) in the kidney.

AA reduced renal Klotho protein expression.

Finally, we examined the expression of antiaging proteins in the kidney of the vehicle control and AA groups. Klotho was significantly decreased in the kidney of the AA group compared with the vehicle control group (Fig. 6A). In contrast, renal expressions of nicotinamide phosphoribosyltransferase (NAMPT) and SIRT1 were not different between the vehicle control and AA groups (Fig. 6B and C).

Discussion

The present study is the first to focus on evaluation of renal aging-associated alterations in AAN using markers of senescence such as p16 and SA-β-gal activity. AA treatment promoted renal atrophy, tubulointerstitial fibrosis, and renal functional decline, accompanied by upregulation of renal p16 mRNA and SA-β-gal-positive staining. Furthermore, the AA group demonstrated features of renal aging-related mechanisms such as mitochondrial abnormalities, increased oxidative stress, and downregulation of the antiaging gene, Klotho. Taken together, our observations suggest that chronic AA stimulation partially mimics renal aging.

Cellular senescence is a process that imposes permanent proliferative arrest on cells in response to various stressors such as DNA damage. It makes potentially important contributions to aging and age-related diseases. Expression of p16, a cyclin-dependent kinase inhibitor, correlates with aging in various organs[6]. Renal expression of p16 in 26-month-old mice was reportedly over 10 times that in 2.5-month-old mice. Calorie restriction that is a stimulation to lengthen lifespan also blunt expression of p16 in various organs including the kidney. Additionally, in INK-ATTAC mice, apoptosis-induced elimination of p16-expressing senescent cells via injection of AP20187, a FK506-binding protein dimerizer[7], attenuates features of renal aging such as glomerular sclerosis and renal functional decline. Therefore, p16 is one of the most important senescence-related factors. Senescent cells can be detected by SA-β-gal staining, which reveals increased β-galactosidase activity at pH 6.0[8]. SA-β-gal is also one of the most widely used biomarkers of senescent and aging cells. Renal mRNA expression of p16 is increased in aged rat kidneys and is accompanied by increased SA-β-gal activity in renal epithelium[9]. In the present study, we identified upregulation of renal p16 mRNA and SA-β-gal-staining positivity, which indicate that AA induces renal senescence. GLS was recently reported to be essential for survival of senescent cells, in which GLS expression is induced to enhance glutaminolysis and neutralize intracellular pH[10]. Inhibition of GLS-dependent glutaminolysis in aged mice was shown to specifically eliminate senescent cells and ameliorate age-associated organ dysfunction. In the present study, upregulation of renal GLS mRNA

indicated accumulation of senescent cells in the kidney of the AA group. Collectively, chronic AA administration caused cellular senescence in the kidney.

Along with cellular senescence, mitochondrial dysfunction is an essential mechanism underlying age-associated tissue damage, and is accompanied by accumulation of ROS[11,12]. Cellular senescence is closely associated with mitochondrial dysfunction. Mitochondrial dysfunction drives and maintains cellular senescence[13]. Simultaneously, cellular senescence contributes directly to mitochondrial dysfunction[14]. Bnip3 is localized primarily in the outer mitochondrial membrane and may play a role in regulation of mitophagy in cultured renal proximal tubular cells in response to oxidative stress and hypoxia. Bnip3 expression in renal tubules is increased under renal ischemia-reperfusion injury (IRI) in mice, and Bnip3 knockout mice demonstrate aggravated renal IRI. In aged mice, calorie restriction increases autophagy activity in tubular cells via upregulation of Bnip3, and improves age-degenerated renal functions[15]. In the present study, electron microscopic observation revealed features of mitochondrial abnormalities that may be affected by reduced renal Bnip3 expression or cellular senescence. Mitochondria are the main intracellular source of ROS. To assess the effects of accumulation of abnormal mitochondria on renal ROS status, we examined renal accumulation of 4-HNE and showed that AA induced ROS accumulation in the kidney. NADPH oxidases are also known for being major source of ROS. During the acute phase of AAN in the mouse model, renal expression of Nox2 mRNA is elevated, and is associated with reduction in nitric oxide availability linked to sustained hypoxia and ischemic insult[16]. In aged rat kidney, ROS increases are accompanied by increased expression of Nox2[17]. These findings suggested that AA may induce age-related phenotypes through accumulation of ROS via dysfunctional mitochondria and upregulation of NADPH oxidases.

Klotho gene expression was decreased in the kidney of the AA group, although the expressions of NAMPT and SIRT1 were unaltered. Klotho is an antiaging gene that encodes a single-pass transmembrane protein, which serves as an aging suppressor. The aging process in Klotho-deficient mice resembles that of humans, including short lifespan, infertility, arteriosclerosis, skin atrophy, osteoporosis, and emphysema[18]. Klotho mutant mice also exhibit a phenotype of accelerated aging, which is restored by p16 ablation[19]. Therefore, Klotho is an important factor in aging, and Klotho gene-modified mice have been widely used in research on aging. However, Klotho gene-modified mice may be inappropriate for research on renal aging owing to systemic age-associated impairments and the fact that renal function is unaffected (i.e., creatinine levels). In contrast, models of AAN may be used as a drug-induced model of renal aging for research purposes, and boast the following advantages: relative ease of implementation, and allows for estimation of the effects of interventions on renal functional decline.

The present study had limitations. We evaluated phenotypes of aging with main focus on cellular senescence, mitochondrial morphology, and aging-related gene expression. However, mechanisms of aging are much more complex than the points we examined and remain incompletely understood. Additionally, although Klotho gene expression was decreased in response to AA, we could not demonstrate a causal relationship with these pathological changes of AAN. Therefore, further studies are

necessary to reveal how the molecules plays a role against development of AAN in the model. Nonetheless, the present study provides a novel insight in that AAN may be useful as a model of renal aging. It is important to note that phenotypic changes in the kidney can strongly affect lifespan. Although the kidney is easily affected by aging-associated changes, inhibition of renal aging can lengthen overall lifespan. Therefore, further research on renal aging using models of AAN may lead to increased longevity in the future.

Methods

Animals

This study was performed in accordance with the National Institutes of Health guidelines for the use of experimental animals. All animal experiments were reviewed and approved by the Animal Studies Committee of Yokohama City University (Approval Number: FA20-027), and were conducted in compliance with ARRIVE guidelines. Efforts were made to minimize the number of animals used and to minimize suffering. Mice were housed in a controlled environment with 12-h light/dark cycle at temperature of 25°C. Mice were allowed free access to food and water.

Eight-week-old male C57BL/6 mice were purchased from Charles River Laboratories and assigned to the AA or vehicle control group after 1-week acclimatization. Mice were intraperitoneally administered AA (3 mg/kg) (Aristolochic acid I; Sigma-Aldrich, St. Louis, MO, USA) or vehicle (75% dimethyl sulfoxide) twice per week for 4 weeks, followed by a 4-week recovery period.

Blood pressure measurement

Systolic blood pressure and heart rate were measured using the tail-cuff method (BP-Monitor MK-2000; Muromachi Kikai Co., Tokyo, Japan), as previously described[20,21]. All measurements were performed between 9:00–14:00 h. At least 10 measurements were performed in each mouse and the mean value was used for analysis.

Real-time quantitative reverse transcription polymerase chain reaction analysis

Total RNA was extracted from renal tissue using ISOGEN (Nippon Gene, Tokyo, Japan); cDNA was synthesized using the SuperScript III First-Strand System (Invitrogen, Carlsbad, CA, USA). Real-time quantitative reverse transcription polymerase chain reaction analysis was performed using a CFX96 Touch Real-Time PCR Detection System (Bio Rad, Hercules, CA, USA); reverse transcription products were incubated with TaqMan PCR Master Mix and a custom TaqMan probe (Applied Biosystems, Foster City, CA, USA), as previously described[22]. The following TaqMan probes were used: Collagen I (Mm00801666_g1), Collagen III (Mm01254476_m1), TGF-β (Mm01178819_m1), p53 (Mm00441964_g1), p21 (Mm04205640_g1), p16 (Mm00494449_m1), GLS (Mm01257297_m1), Bnip3 (Mm01275600_g1), and Nox2 (Mm00627011_m1). mRNA levels were normalized to those of the 18S rRNA control.

Western blot analysis

Protein expression was analyzed using western blot of tissue homogenates, as previously described[23,24]. Briefly, total protein extracts were prepared from tissue with sodium dodecyl sulfate-containing sample buffer. Protein concentration of each sample was measured with a Detergent-Compatible Protein Assay Kit (Bio-Rad, Hercules, CA, USA) and a NanoDrop One (Thermo Fisher Scientific, Waltham, MA, USA) using bovine serum albumin as the standard. Equal amounts of protein extract from tissue samples were fractionated on 5–20% polyacrylamide gels (ATTO, Tokyo, Japan). Separated proteins were then transferred to polyvinylidene difluoride membranes using a Semi-Dry Transfer System (ATTO, Tokyo, Japan). Membranes were blocked for 1 h at room temperature with phosphate-buffered saline containing 5% skim milk powder. Membranes were incubated with primary antibodies against Klotho (ab181373 1:1000, Abcam, Cambridge, MA, USA), NAMPT (sc-67020 1:5000, Abcam, Cambridge, MA, USA), SIRT1 (07-131 1:1000, Merck Millipore, Burlington, MA, USA), 4-HNE (MHN-100P 1:1000, JaICA, Fukuroi, Japan), and GAPDH (2118, 1:2000, Cell Signaling Technology, Danvers, MA, USA). Membranes were washed and incubated with secondary antibodies for 60 min at room temperature. The sites of antibody-antigen reactions were visualized using enhanced chemiluminescence substrate (Merck, Kenilworth, NJ, USA). GAPDH was used as the loading control. Images were analyzed quantitatively using a ChemiDoc Touch (Bio Rad, Hercules, CA, USA).

Histological analysis

Histological analysis was performed as previously described[25]. Mouse renal tissues were fixed with 4% paraformaldehyde and subsequently embedded in paraffin. Sections (4-μm thick) were stained with PAS and Masson's trichrome. To evaluate glomerular area, 50 glomeruli per mouse were measured and averaged. All images were acquired using a BZ-9000 microscope (Keyence, Osaka, Japan).

SA-β-gal staining

Renal tissues from mice were rapidly frozen on dry ice, and mounted in O.C.T. Compound (Sakura Finetek Japan, Tokyo, Japan). Sections (4-μm thick) were prepared using a cryostat (HM550-VPD; Thermo Fisher Scientific, Waltham, MA, USA), and mounted onto glass slides. SA-β-gal activity was measured using a senescence detection kit (BioVision, Milpitas, CA, USA) according to the manufacturer’s protocol. Samples were viewed under bright field at ×100 magnification using a BZ-9000 microscope (Keyence, Osaka, Japan).

Electron microscopy analysis

Electron microscopy analysis was performed as previously described[26]. Briefly, mice were anesthetized with isoflurane and perfused through the right aortic arch with heparinized (5 U/mL) physiological saline and 2.5% glutaraldehyde in 0.1 mol/L phosphate buffer at pH 7.4. Specimens for transmission electron microscopy were immersed in 1% osmium tetroxide for 2 h, dehydrated in an ethanol series, and embedded in an Epon mixture. Ultrathin sections were stained for electron microscopy with uranyl acetate and lead citrate, and examined using a Hitachi H-7500 transmission electron microscope operated at 80

kV (Hitachi, Ltd, Tokyo, Japan). Observations were at ×5000 and photographed with a charge-coupled device camera.

Biochemical analysis

Blood samples were collected by cardiac puncture in the fed state. Whole blood samples were centrifuged at 3000 rpm (MR-150, Tomy Seiko Co., Ltd., Tokyo, Japan) for 10 min at 4°C to separate plasma. The resulting plasma samples were stored at − 80°C until use. Plasma creatinine, blood urea nitrogen, and urinary creatinine levels were measured using a Hitachi 7180 autoanalyzer (Hitachi, Tokyo, Japan).

Statistical analysis

Statistical analyses were performed using GraphPad Prism software (GraphPad Software, La Jolla, CA, USA). Data are presented as mean ± standard error of the mean. Unpaired *t*-tests were used to determine differences between the AA and vehicle control groups. $P < 0.05$ was considered statistically significant.

Declarations

CONFLICT OF INTEREST

The authors declare no competing interests.

AUTHOR CONTRIBUTIONS

S.U. and H.W. designed and conducted the study. S.U., H.W., and K.A. wrote the manuscript. S.U., H.W., K.A., T.Y., T.S., E.A., S.T., S.T., S.T., S.K., K.U., T.K., and Y.A. performed experiments. S.U., H.W., and K.A. analyzed data. K.F., A.Y., and K.T. supervised the study. All authors approved the final manuscript.

ACKNOWLEDGEMENTS

This work was supported by grants from the Yokohama Foundation for Advancement of Medical Science; the Uehara Memorial Foundation; the Japan Kidney Association-Nippon Boehringer Ingelheim Joint Research Program; the Japan Society for the Promotion of Science; the Japanese Association of Dialysis Physicians; the Salt Science Research Foundation (20C4); and the Strategic Research Project of Yokohama City University.

Source of Funding

None.

Conflicts of Interest

None.

References

1. Ebert, N. et al. Prevalence of reduced kidney function and albuminuria in older adults: the Berlin Initiative Study. *Nephrol Dial Transplant.* **32**, 997-1005 (2017).
2. O'Sullivan, ED. et al. Renal Aging: Causes and Consequences. *J Am Soc Nephrol.* **28,** 407-420. (2017).
3. Vanhooren, V. et al. The mouse as a model organism in aging research: usefulness, pitfalls and possibilities. *Ageing Res Rev.* **12,** 8-21 (2017).
4. Kuro-o, M. et al. Mutation of the mouse klotho gene leads to a syndrome resembling ageing. **390,** 45-51 (1997).
5. Schmeiser, HH. et al. DNA adduct formation of aristolochic acid I and II in vitro and in vivo. **9,** 297-303 (1988).
6. Krishnamurthy, J. et al. Ink4a/Arf expression is a biomarker of aging. *J Clin Invest.* **114,** 1299-1307 (2004).
7. Baker, DJ. et al. Naturally occurring p16(Ink4a)-positive cells shorten healthy lifespan. **530,** 184-189 (2016).
8. Dimri, GP. et al. A biomarker that identifies senescent human cells in culture and in aging skin in vivo. *Proc Natl Acad Sci USA*. **92,** 9363-9367 (1995).
9. Melk, A. et al. Cell senescence in rat kidneys in vivo increases with growth and age despite lack of telomere shortening. *Kidney Int.* **63,** 2134-2143 (2003).
10. Johmura, Y. et al. Senolysis by glutaminolysis inhibition ameliorates various age-associated disorders. **371,** 265-270 (2021).
11. Sun, N. et al. The Mitochondrial Basis of Aging. *Mol Cell*. **61,** 654-666 (2016).
12. Perez-Campo, R. et al. The rate of free radical production as a determinant of the rate of aging: evidence from the comparative approach. *J Comp Physiol B.* **168,** 149-158 (1998).
13. Correia-Melo, C. et al. Mitochondria are required for pro-ageing features of the senescent phenotype. *EMBO J.* **35,** 724-42 (2016).
14. Passos, JF. et al. Feedback between p21 and reactive oxygen production is necessary for cell senescence. *Mol Syst Biol.* **6,** 347 (2010).
15. Kume, S. et al. Calorie restriction enhances cell adaptation to hypoxia through Sirt1-dependent mitochondrial autophagy in mouse aged kidney. *J Clin Invest*. **120,** 1043-1055 (2010).
16. Declèves, AÉ. et al. Protective effect of nitric oxide in aristolochic acid-induced toxic acute kidney injury: an old friend with new assets. *Exp Physiol.* **101,** 193-206 (2016).
17. Zuo, Z. et al. Aging-related kidney damage is associated with a decrease in klotho expression and an increase in superoxide production. *Age (Dordr)* **33,** 261-274 (2011).
18. Kuro-o, M. et al. Klotho as a regulator of oxidative stress and senescence. *Biol Chem.* **389,** 233-241 (2008).
19. Sato, S. et al. Ablation of the p16(INK4a) tumour suppressor reverses ageing phenotypes of klotho mice. *Nat Commun.* **6,** 7035 (2015).

20. Shigenaga, A. et al. Effect of olmesartan on tissue expression balance between angiotensin II receptor and its inhibitory binding molecule. *Hypertension*. **52,** 672–678 (2008).
21. Azushima, K. et al. Effects of rikkunshito on renal fibrosis and inflammation in angiotensin II-infused mice. *Sci Rep.* **9,** 6201 (2019).
22. Wakui, H. et al. Enhanced angiotensin receptor-associated protein in renal tubule suppresses angiotensin-dependent hypertension. **61,** 1203-1210 (2013).
23. Ohki, K. et al. Angiotensin II type 1 receptor-associated protein inhibits angiotensin II-induced insulin resistance with suppression of oxidative stress in skeletal muscle tissue. *Sci Rep*. **8,** 2846 (2018).
24. Azushima, K. et al. Adipocyte-specific enhancement of angiotensin II type 1 receptor-associated protein ameliorates diet-induced visceral obesity and insulin resistance. *J Am Heart Assoc.* **6,** e004488 (2017).
25. Ohsawa, M. et al. Deletion of the angiotensin II type 1 receptor-associated protein enhances renal sodium reabsorption and exacerbates angiotensin II-mediated hypertension. *Kidney Int*. **86,** 570-581 (2014).
26. Takeda, A. et al. Axonal regeneration through the fibrous scar in lesioned goldfish spinal cord. **284,** 134-152 (2015).

Figures

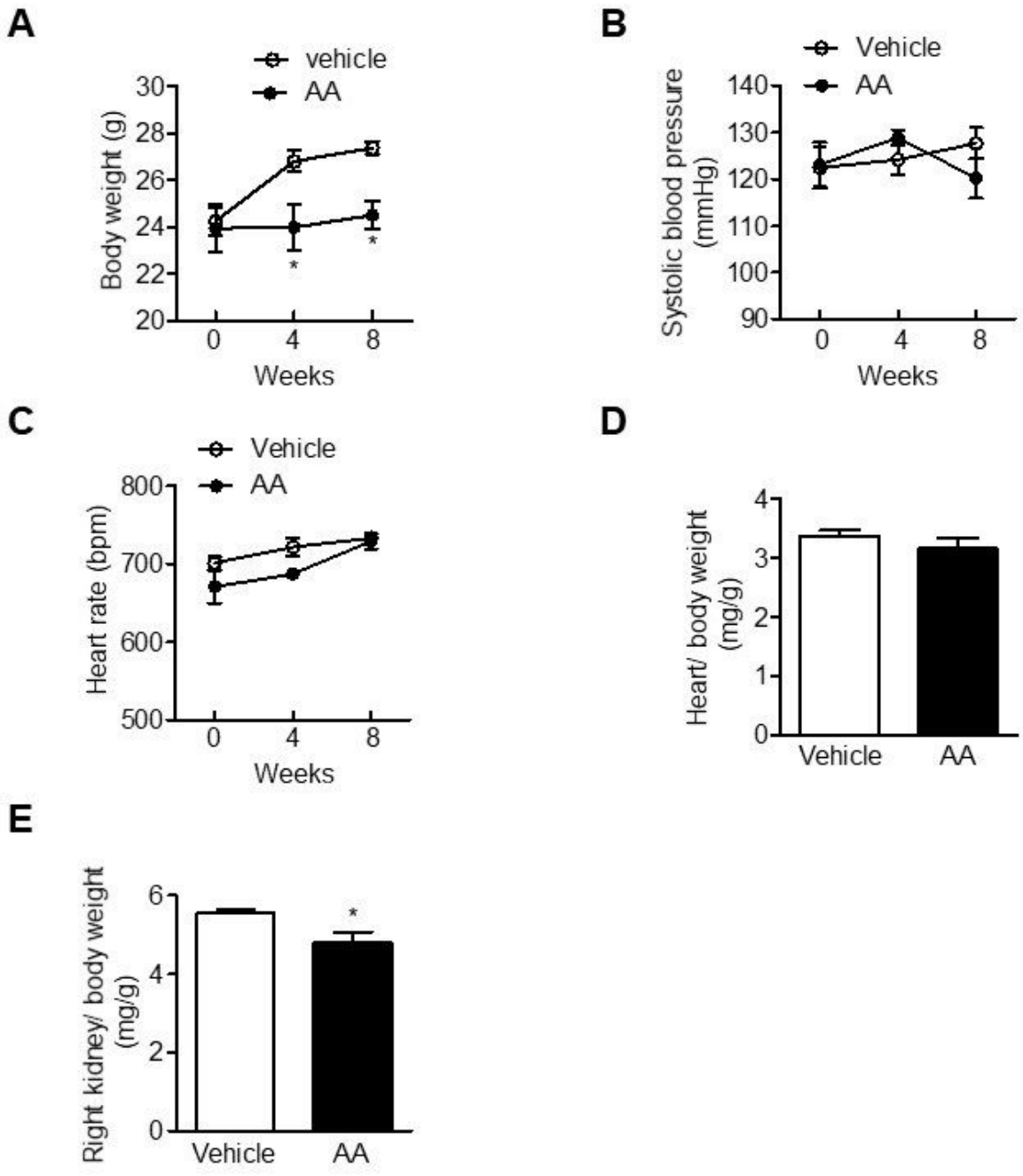

Figure 1

Effects of AA treatment on body weight, systolic blood pressure, heart rate, and tissue weight. (A) Body weight changes in the vehicle and AA groups. (B) Systolic blood pressure and (C) heart rate in the vehicle and AA groups at 0, 4, or 8 weeks after treatment. (D) Heart weight/body weight and (E) kidney weight/body weight ratios in the vehicle and AA groups. (A, B, and C) *P < 0.05 vs. vehicle group. Data are presented as mean ± standard error of the mean (SEM) (n = 5 per group) and analyzed using two-way

repeated measures ANOVA with Bonferroni's post-test. (D and E) *P < 0.05 vs. vehicle group. Data are presented as mean ± SEM (n = 4–5 per group) and analyzed using the unpaired Student's t-test. AA, aristolochic acid.

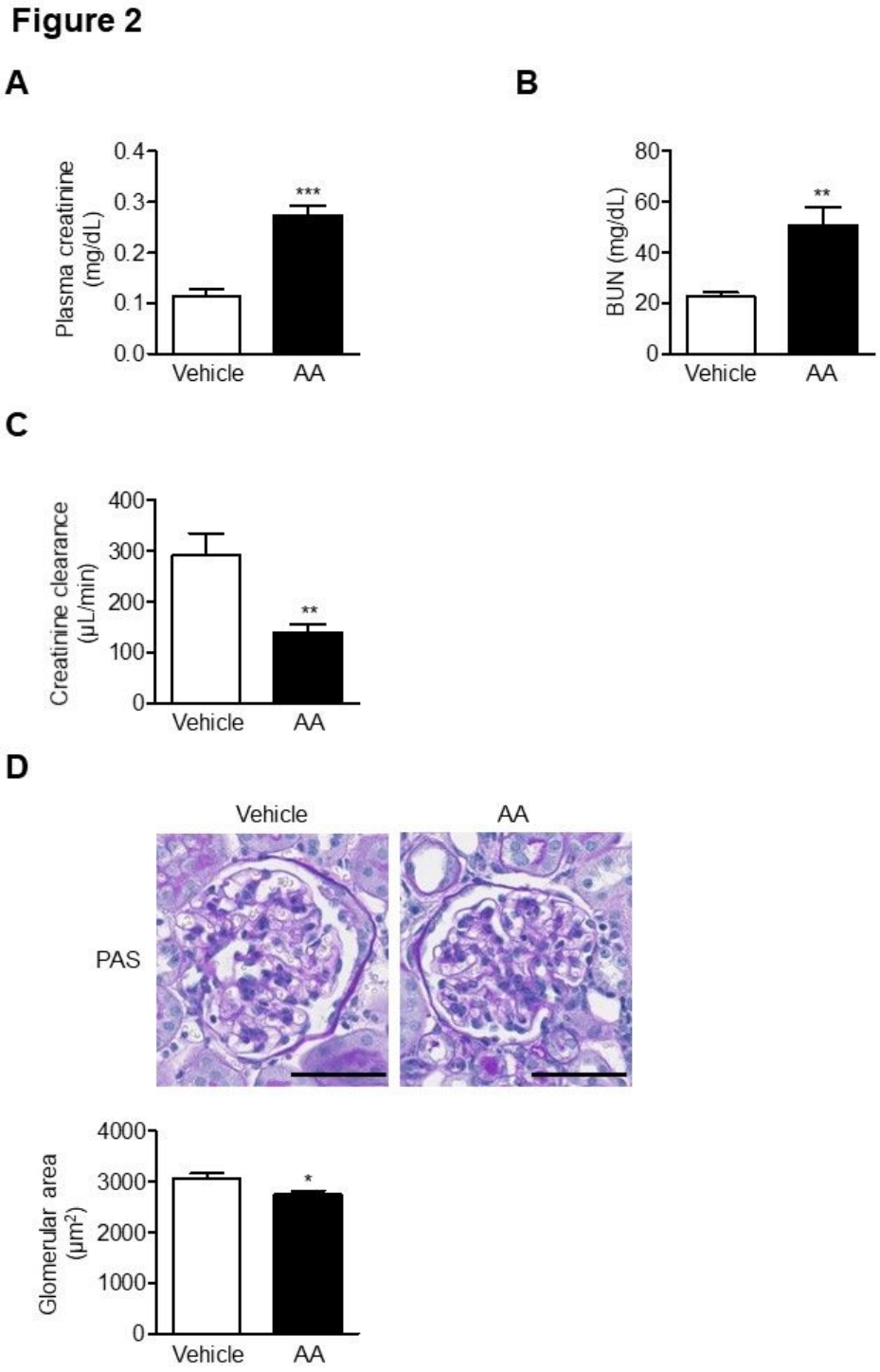

Figure 2

Effects of AA treatment on renal function and pathological changes in glomeruli (A) Plasma creatinine level, (B) BUN, and (C) creatinine clearance were measured in the vehicle and AA groups. (D)

Representative images of PAS-stained kidney sections (bar, 50 μm) and the glomerular area in the vehicle and AA groups. (A, B, C, and D) *P < 0.05, **P < 0.01, ***P < 0.001 vs. vehicle group. Data are presented as mean ± SEM (n = 4–5 per group) and analyzed using the unpaired Student's t-test. AA, aristolochic acid; BUN, blood urea nitrogen; PAS, periodic acid-Schiff.

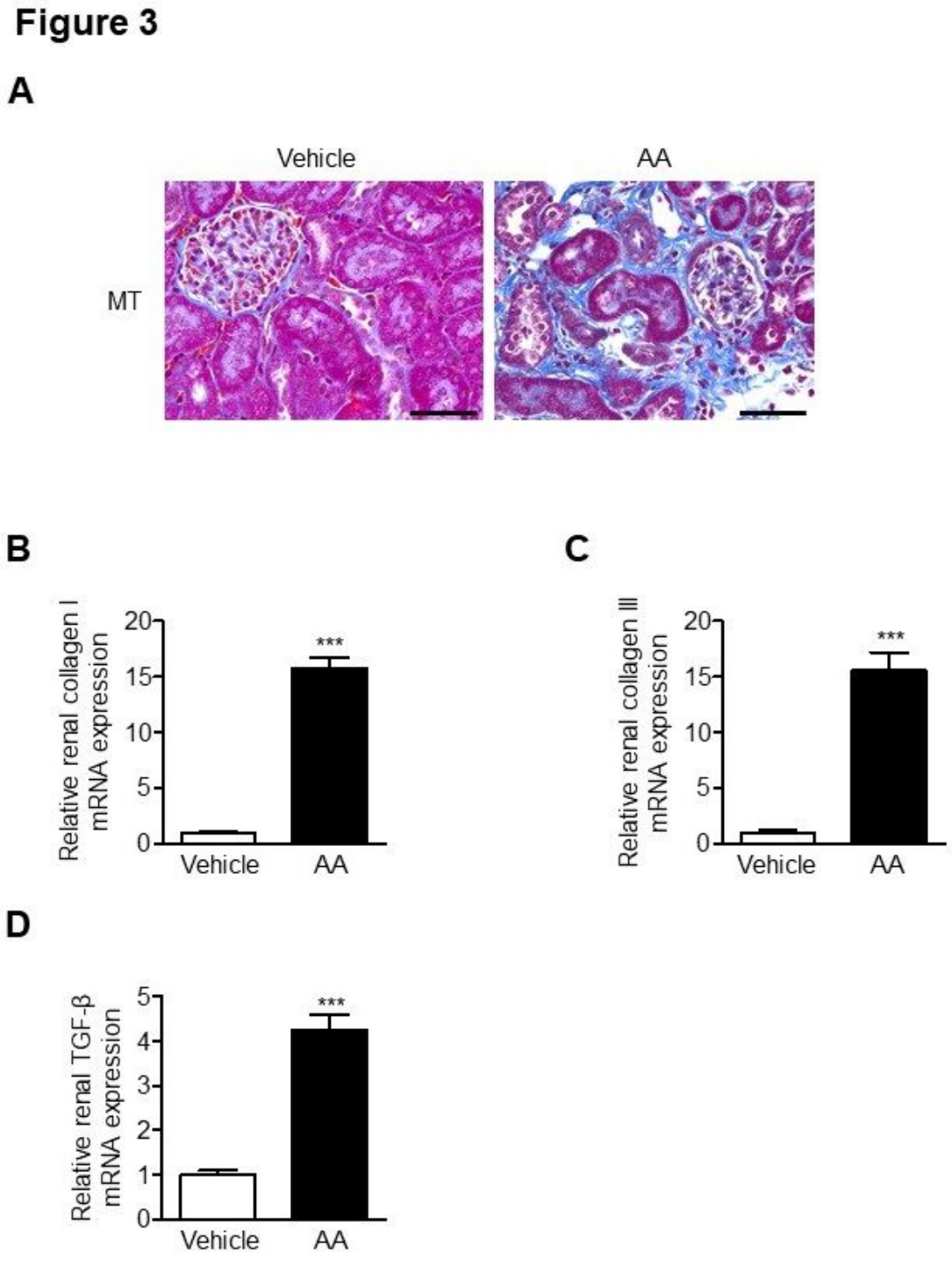

Figure 3

Effects of AA treatment on renal pathological alterations assessed using Masson's trichrome stain and fibrosis-associated gene expression (A) Representative images of MT-stained kidney sections in the vehicle and AA groups (bar, 50 μm). Relative renal mRNA expression of (B) collagen I, (C) collagen III, and (D) TGF-β in the vehicle and AA groups. (B, C, and D) ***P < 0.001 vs. vehicle group. Data are presented as mean ± SEM (n = 5 per group) and analyzed using the unpaired Student's t-test. AA, aristolochic acid; MT, Masson's trichrome; TGF-β, transforming growth factor-β.

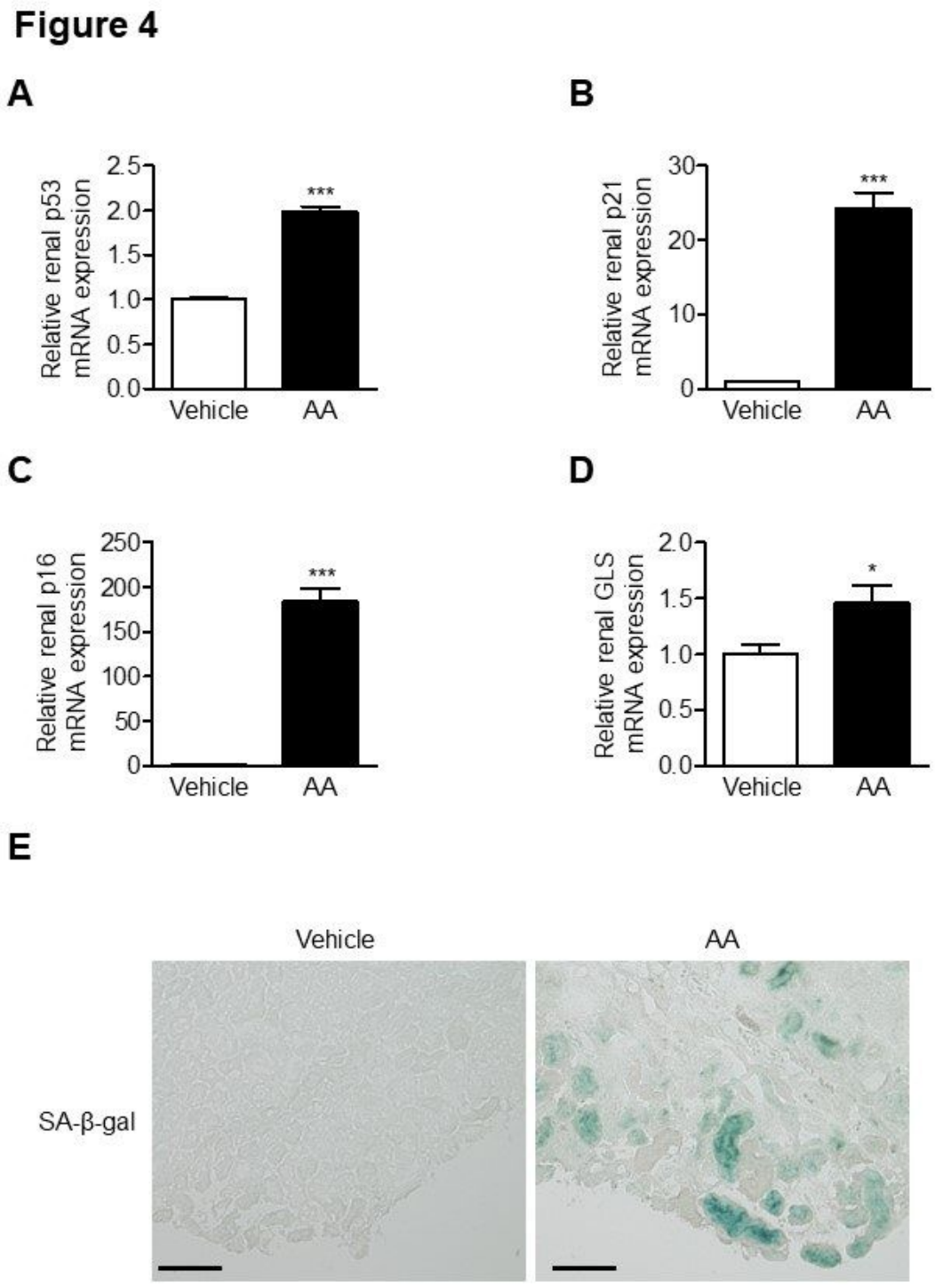

Figure 4

Effects of AA treatment on renal cellular senescence Relative renal mRNA expression of (A) p53, (B) p21, (C) p16, and (D) GLS. (E) Representative images of SA-β-gal-stained kidney sections in the vehicle and AA groups (bar, 100 μm). (A, B, and C) ***P < 0.001 vs. vehicle group. Data are presented as mean ± SEM (n = 5 per group) and analyzed using the unpaired Student's t-test. AA, aristolochic acid; GLS, glutaminase; SA-β-gal; senescence-associated β-galactosidase.

Figure 5

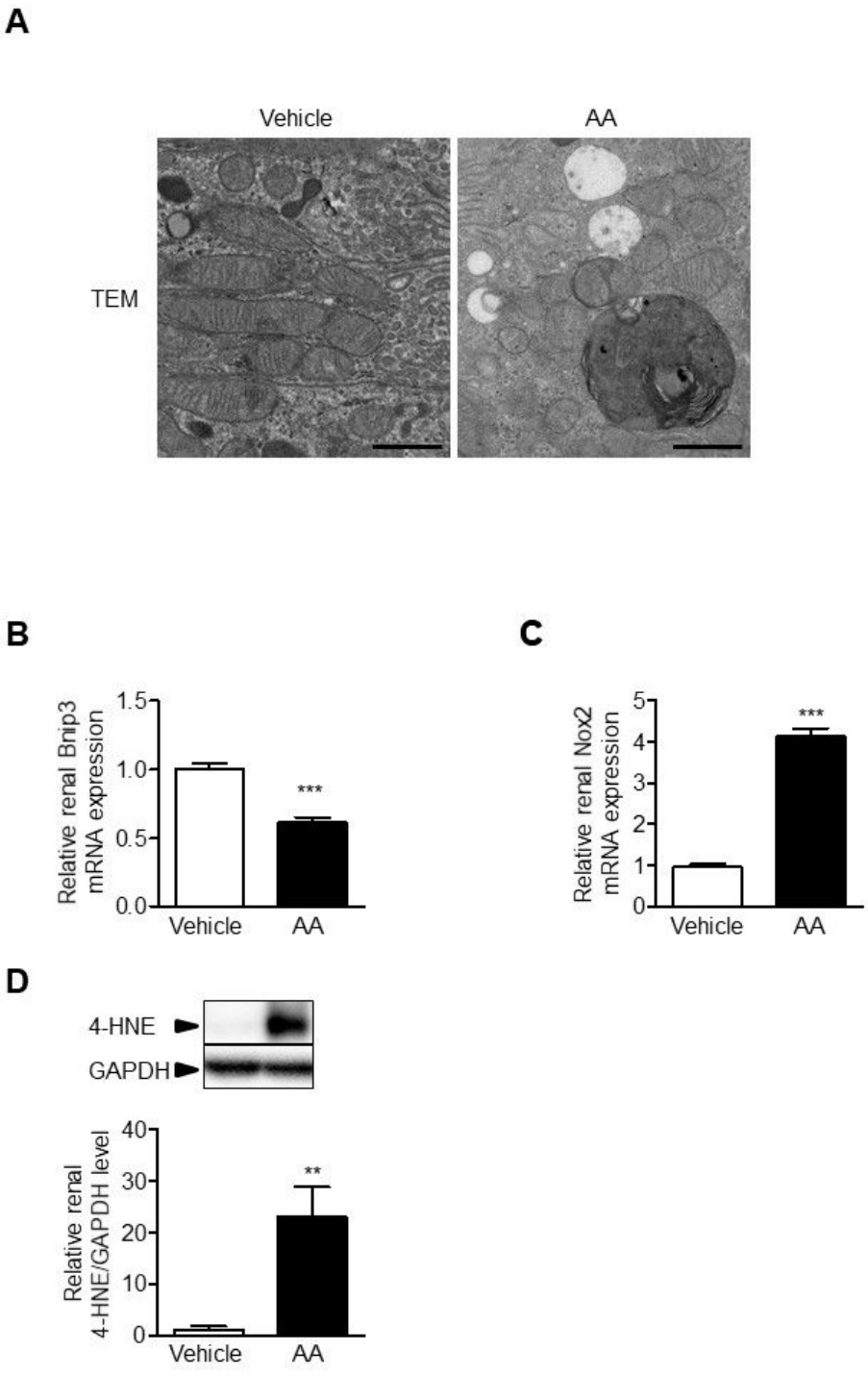

Figure 5

Effects of AA treatment on proximal tubular cells and ROS (A) Representative TEM images of proximal tubular cells in the kidney of the vehicle and AA groups (original magnification, ×5000, bar, 1 μm). Relative renal mRNA expression of (B) Bnip3 and (C) Nox2 in the vehicle and AA groups. (D) Relative renal 4-HNE level in the vehicle and AA groups. (B, C, and D) **P < 0.01, ***P < 0.001 vs. vehicle group. Data are presented as mean ± SEM (n = 5 per group) and analyzed using the unpaired Student's t-test. AA, aristolochic acid; TEM; transmission electron microscope, Bnip3, BCL2/adenovirus E1B 19-kDa interacting protein 3; 4-HNE; 4-hydroxy-2-nonenal.

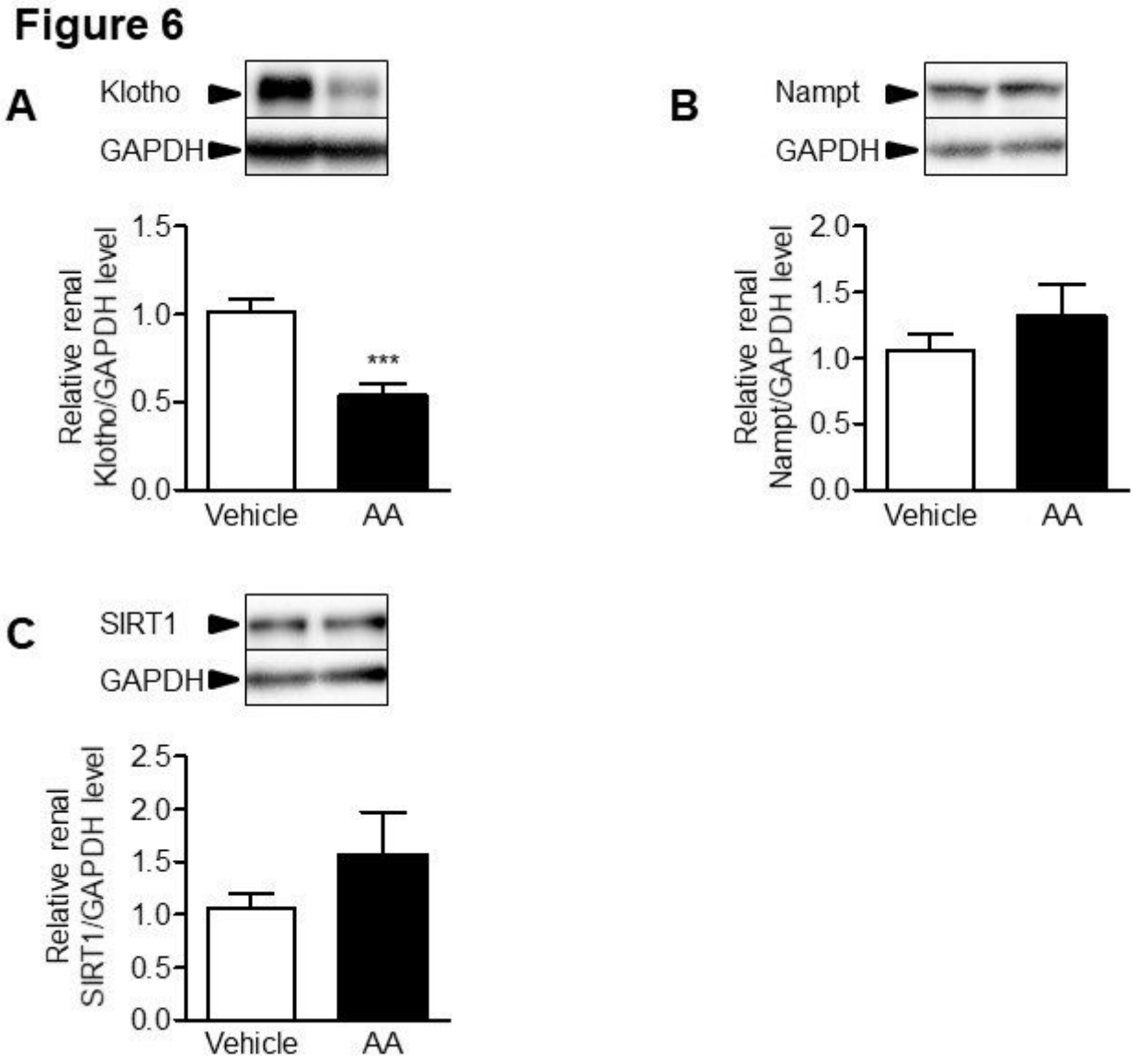

Figure 6

Effects of AA treatment on renal expression of antiaging proteins (A, B, and C) Relative renal protein expression of Klotho, NAMPT, and SIRT1 in the vehicle and AA groups. (A, B, and C) ***P < 0.001 vs.

vehicle group. Data are presented as mean ± SEM (n = 5 per group) and analyzed using the unpaired Student's t-test. AA, aristolochic acid; NAMPT, Nicotinamide phosphoribosyltransferase.

Supplementary Files

This is a list of supplementary files associated with this preprint. Click to download.

- UrateSRmaintext.docx